Research Square

Preprints are preliminary reports that have not undergone peer review.
They should not be considered conclusive, used to inform clinical practice,
or referenced by the media as validated information.

SST-Gradient Driven Asymmetric Decline of Coastal Wind Power in Northwest Africa: Multi-Model Attribution and Projections to 2100

Y. S. Badry[1]

Yousry.Saad.Badry@faps.cu.edu.eg

Cairo University

El-Sayed. M. Robaa[2]

Cairo University

F. I. Moursy[3]

Cairo University

Mustafa A. Mohamed[4]

Cairo University

Article

Keywords: Wind power density, climate change attribution, SST gradient, constrained projections, renewable energy resilience, North Africa, CMIP6, multi-model ensemble

Posted Date: November 13th, 2026

DOI: https://doi.org/10.21203/rs.3.rs-10018519/v1

License: This work is licensed under a Creative Commons Attribution 4.0 International License.
Read Full License

Additional Declarations: No competing interests reported.

Major Revision

SST-Gradient Driven Asymmetric Decline of Coastal Wind Power in North-west Africa: Multi-Model Attribution and Projections to 2100

Y. S. Badry[1], El-Sayed. M. Robaa[2], F. I. Moursy[3], Mustafa A. Mohamed[4]

[1] Department of Natural Resources (Meteorology), Faculty of African Postgraduate Studies, Cairo University,12613 Giza, Egypt.
Yousry.Saad.Badry@faps.cu.edu.eg
[2] Astronomy, Space Science and Meteorology Department, Faculty of Science - Cairo University, 12613, Giza, Egypt. robaa@sci.cu.edu.eg
[3] Department of Natural Resources (Meteorology), Faculty of African Postgraduate Studies, Cairo University,12613 Giza, Egypt.
Fawzya.moursy@cu.edu.eg
[4] Department of Natural Resources (Meteorology), Faculty of African Postgraduate Studies, Cairo University,12613 Giza, Egypt Mostafa_elhameed@cu.edu.eg

Corresponding Author: Y. S. Badry

Abstract

This study quantifies the asymmetric decline in wind power density along Morocco's Mediterranean and Atlantic coasts and develops a multi-model projection framework. Analysis of ERA5 reanalysis data (1981–2020), evaluated against independent NASA POWER, MERRA-2, and NOAA OISST datasets, reveals a pronounced north–south contrast: the southern coast exhibits wind power density approximately 1.6 times higher than the northern coast, whereas the northern region shows 1.9 times greater inter-annual variability and an 11% faster rate of decline. A Random Forest attribution model identifies the Mediterranean–Canary Current sea-surface-temperature gradient as a dominant predictor of the north–south wind-speed differential, with the two SST predictors accounting for approximately 68% of the total permutation importance. The statistical relationship is consistent with a physical mechanism involving differential ocean warming and associated changes in the regional pressure gradient. Comparative analysis of constrained linear, logistic, quadratic, and CMIP6-informed projection approaches indicates that methodological choice introduces a 10–20-year range in projected threshold-crossing times. Five CMIP6 models were used to characterize structural model uncertainty under SSP1-2.6, SSP2-4.5, and SSP5-8.5. The results indicate substantially earlier loss of the 150 W m^{-2} viability threshold in the northern region than in the southern region, although the precise crossing time depends strongly on the projection method and emissions scenario. These findings highlight the importance of physically informed, multi-model approaches for assessing climate-related risks to coastal wind-energy resources in Morocco.

Keywords: Wind power density; climate change attribution; SST gradient; constrained projections; renewable energy resilience; North Africa; CMIP6; multi-model ensemble

1. Introduction

Morocco's renewable energy strategy targets 52% of installed electricity capacity from renewable sources by 2030 [1], relying heavily on wind resources along the Atlantic and Mediterranean coastlines [23]. Previous assessments of Morocco's offshore wind resource have highlighted its theoretical potential but did not account for climate-induced long-term trends [24]. The long-term viability of this strategy is increasingly intertwined with anthropogenic climate change, which alters regional atmospheric circulation patterns. Although global "terrestrial stilling" has been documented [2], regional wind responses exhibit substantial heterogeneity and are strongly influenced by localized air–sea interactions [3].

In Northwest Africa, a key climatic regulator is the meridional sea surface temperature (SST) gradient between the rapidly warming Mediterranean Sea [4] and the relatively stable, upwelling-cooled Canary Current system. This SST contrast modulates the regional pressure field and coastal wind regimes upon which Morocco's wind energy sector critically depends [5].

Existing climate impact assessments frequently rely on simplistic linear extrapolations or isolated global climate model outputs. Such approaches can yield physically implausible projections or fail to capture region-specific, nonlinear atmospheric dynamics [3], creating a critical disconnect between climatological research and actionable energy policy.

To address these gaps, this study pursues three objectives. First, wind speed and wind power density differences between the two coasts are quantified and validated using ERA5 data cross-checked against independent NASA and NOAA products. Second, the drivers of these differences are identified—specifically, whether the SST gradient between the Mediterranean Sea and the Canary Current constitutes the suspected controlling mechanism. Third, rather than extrapolating trends linearly (which yields physically implausible values by 2100), multiple projection models are developed to quantify how methodological choice influences planning timelines. The underlying hypothesis is that differential warming weakens the pressure gradient, thereby disproportionately impacting the northern coast. Furthermore, because no single model is perfect, an ensemble approach provides a more realistic characterization of future risks for both researchers and energy planners.

---

2. Data and Methods

2.1 Study Region and Data Sources

The study focuses on two distinct coastal sectors of Morocco (Figure 1):

- **Northern Mediterranean zone (35.6–35.8°N):** This zone centers on the Tanger I (140 MW), Tanger II (200 MW), Tetouan I (54 MW), and Koudia Al Baida (200 MW) wind farm complexes, which represent 594 MW of operational and in-progress capacity. These

sites are influenced by complex flows through the Strait of Gibraltar and Mediterranean synoptic systems.

- **Southern Atlantic zone (27.9–28.0°N):** This zone focuses on the Tarfaya (301 MW) and Akhfener (200 MW) wind farms, which constitute 501 MW of operational capacity. These sites are characterized by strong, persistent Atlantic trade winds anchored to the Canary Current system.

The parent study analyses twelve wind farm sites distributed across four regions of Morocco [6, 26, Ch. 3, Table 3.1]: **Southern Coastal** (Tarfaya, Akhfener), **Central Coastal** (Essaouira, El-Oualidia), **Northern Coastal** (Tanger I, Tanger II, Tetouan I, Koudia Al Baida, Haouma, Jbel Khelladi), and **Inland** (Taza, Midelt). The primary scientific focus of the present paper is the northern-versus-southern coastal contrast, which forms the basis of the attribution and projection analyses in Sections 3.3, 3.4, and 4.1. The Central Coastal and Inland regions are retained in the uncertainty decomposition (Section 3.5, Table 4) for completeness of the wider site network, but they are not part of the primary northern-versus-southern comparison.

For the baseline period 1981–2020, we extracted monthly mean 100 m wind speed and sea surface temperature from the ERA5 reanalysis [6] at the coordinates of these wind farm sites. All ERA5 data used in this study were extracted from the GRIB archive and processed into monthly averages at 100 m height. For the Random Forest attribution (Section 2.3), these monthly means were used directly, with the seasonal cycle retained. For the ERA5 validation (Section 3.1), the monthly means were deseasonalised prior to computing validation statistics. For the CMIP6 projections (Section 2.4), NASA POWER monthly and annual means were used with the seasonal cycle retained.

Justification for using ERA5 reanalysis instead of direct wind park measurements. Direct wind park measurements are often proprietary, have short and incomplete records, and are subject to instrumentation changes or local land-use effects that can create artificial trends. Most selected wind farms were commissioned after 2010 and therefore cannot provide a 1981–2020 baseline. ERA5 provides a homogenised, long-term, spatially consistent record that is essential for climate trend attribution in this context. It should be emphasised that the present study does not perform a comprehensive, direct validation of ERA5 against wind farm measurements. A detailed quantitative comparison with in-situ wind park data was beyond the scope of this study and is identified as a priority for future work.

To ensure the robustness of the ERA5 dataset used here, we validated it against independent, freely available gridded datasets rather than against wind park measurements:

- Wind speed: NASA Prediction of Worldwide Energy Resources (POWER) [7] and MERRA-2 [8]
- Sea surface temperature: NOAA OISST v2.1 [9] and NASA GHRSST Level 4 analysis [10]

Validation employed multiple metrics: Pearson correlation coefficient (R), root mean square error (RMSE), and mean bias error (MBE). All validation statistics were computed on deseasonalised monthly anomalies, in which the seasonal cycle was removed by subtracting the long-term monthly climatology (1981–2020) from each time series. **This step was applied specifically for the model validation to avoid spurious correlations driven by the shared annual cycle; it was not applied to the Random Forest attribution analysis in Section 2.3, which uses monthly mean data at 100 m with the seasonal cycle retained.**

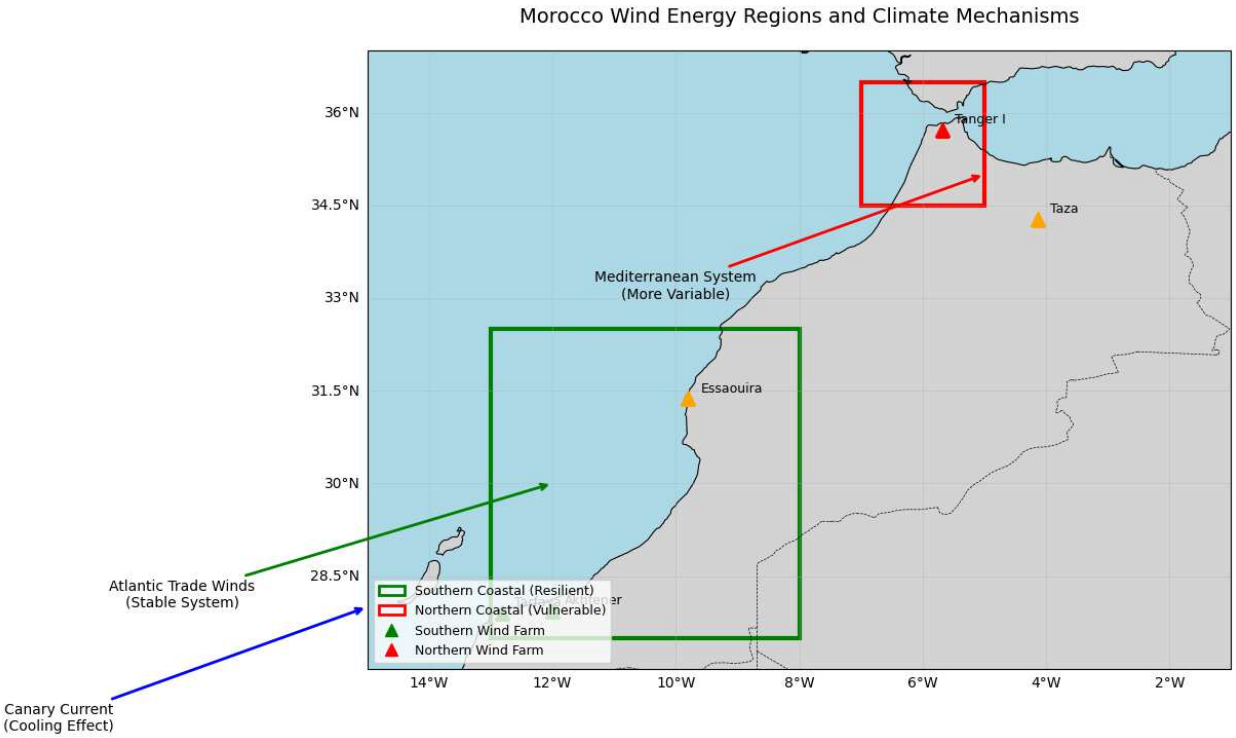


Figure 1. Map of the study area showing the northern Mediterranean zone (red box) and southern Atlantic zone (green box), with major wind farm locations, the Canary Current, and the Mediterranean Sea.

2.2 Trend Analysis and Wind Power Density Calculation

Monotonic trends in wind speed and WPD were identified using the nonparametric Mann–Kendall test [11], with trend magnitudes quantified via Sen's slope estimator [12]. Wind power density was calculated as:

$$WPD = \frac{1}{2}\rho v^3 \qquad (1)$$

where $\rho = 1.225$ kg m^{-3}is standard air density and $v$is the 10 m wind speed [25].

2.3 Machine Learning Attribution

To investigate the statistical predictors of the monthly north–south wind-speed differential (Δv), we implemented a Random Forest regression model [13] using Mediterranean SST, Canary Current SST, and the derived sea-level pressure gradient (ΔP). All predictor and target variables were derived from ERA5 monthly mean data at 100 m with the seasonal cycle retained (1981–2020); no deseasonalisation was applied to the Random Forest inputs. This is distinct from the validation procedure described in Section 3.1, in which deseasonalised anomalies were used solely for model evaluation. The model was trained using 80% of the monthly observations (1981–2012) and evaluated on the remaining 20% (2013–2020). Hyperparameters (100 trees and maximum depth = 5) were selected using five-fold cross-validation within the training period. Predictor importance was quantified using permutation importance. Because the SST predictors are physically and statistically related, permutation importance is interpreted as an indicator of predictive contribution rather than as evidence of independent causal effects.

2.4 Climate Scenarios

Observed trends were projected to 2100 under three Shared Socioeconomic Pathways: SSP1-2.6 (low emissions), SSP2-4.5 (moderate), and SSP5-8.5 (high emissions) [14].

Five CMIP6 models were used for the SST-gradient-informed projections (Table 1). For each model, the use of the first ensemble member (r1i1p1f1) provides a consistent basis for comparing structural differences among the selected climate models, while internal variability is not fully sampled. Model spread was quantified as the standard deviation of projected wind speed changes across the five models and is reported as the model-uncertainty component in the uncertainty decomposition (Section 2.7, Table 4).

Table 1. CMIP6 models used in the SST-gradient-informed projections. Model acronyms follow the CMIP6 standard naming convention. Ensemble member r1i1p1f1 follows the CMIP6 standard notation (realization, initialization, physics, forcing).

Model	Modelling Centre	Experiment	Ensemble	Atmospheric Resolution	Rationale
CESM2	NCAR, USA	ssp126, ssp245, ssp585	r1i1p1f1	~1°	Widely used, detailed Earth-system processes
MPI-ESM1-2-LR	MPI-M, Germany	ssp126, ssp245, ssp585	r1i1p1f1	~1.9°	Strong European performance
UKESM1-0-LL	Met Office, UK	ssp126, ssp245, ssp585	r1i1p1f1	~1.25°	Interactive chemistry and aerosols

Model	Modelling Centre	Experiment	Ensemble	Atmospheric Resolution	Rationale
MIROC6	JAMSTEC, Japan	ssp126, ssp245, ssp585	r1i1p1f1	~1.4°	High-resolution atmosphere/ocean
GFDL-ESM4	NOAA GFDL, USA	ssp126, ssp245, ssp585	r1i1p1f1	~1°	Strong atmosphere/ocean dynamics

2.5 Multi-Model Projection Framework

To avoid reliance on any single method and to quantify the sensitivity of projections to methodological choices, four different approaches were tested. Each captures uncertainty in a different way:

2.5.1 Constrained Linear Model

The simplest method projects the historical trend forward using Sen's slope. However, because unrestricted linear extrapolation eventually yields physically implausible negative wind power densities, a physical lower bound was imposed. The practical minimum wind speed for turbine operation is represented by $L = 50\ \mathrm{W \cdot m^{-2}}$, below which kinetic flux is insufficient for meaningful energy generation. This model provides a first-order baseline warning but assumes stationarity—that past trends reliably indicate future conditions.

$$WPD(t) = \max(WPD_0, +\beta t L) \qquad (2)$$

where $\beta$is the historical Sen's slope and $L = 50\ \mathrm{W \cdot m^{-2}}$is a physical lower bound representing the minimum kinetic flux for turbine operation.

2.5.2 Logistic (Sigmoid) Model

Wind resources typically decline asymptotically as a physical limit is approached, rather than abruptly. Therefore, a logistic (sigmoid) curve was applied:

$$WPD(t) = L + \frac{WPD_0 - L}{1 + \exp[k(t - t_0)]} \qquad (3)$$

where $L$is the same $50\ \mathrm{W \cdot m^{-2}}$floor, $k$governs the decline rate, and $t_0$is the midpoint year when half of the total loss has occurred. This shape represents a system gradually approaching a new climatic equilibrium.

2.5.3 Quadratic Model

The simple quadratic model is more appropriate to use when the decrease is accelerated:

$$WPD(t) = \beta_0 + \beta_1 t + \beta_2 t^2 \qquad (4)$$

A negative and statistically significant ($p < 0.05$) value for $\beta_2$indicates an acceleration of wind resource losses, which would bring viability thresholds forward by approximately 5–10 years relative to linear or logistic projections. In the present analysis, $\beta_2$was negative and significant ($p = 0.03$).

2.5.4 CMIP6-Informed Piecewise Model

The last model tries to correlate what is observed historically and what climate models predict. The attribution studies made it abundantly evident that the SST gradient is important. So the first step is to quantify the historical relationship: for every 1°Cthe gradient changes to show how much the north–south wind difference shifts. That gave sensitive values of the factor (α). The second step was to enter the future SST gradients from five CMIP6 models [15–19] under each SSP. Finally, the analyzed historical wind trend compared to the future changes:

$$North(t) = v_{\text{north,hist}}(t) \times \left(1 + \alpha(\Delta SST(t) - \Delta SST_{1981-2020})\right)$$

where $\alpha$is derived from the historical sensitivity. WPD was recomputed from the adjusted wind speeds.

In this approach, the forecasts are linked to the actual mechanism causes of the entire phenomenon, instead of being essentially statistical.

2.5.5 Justification for the SST-gradient-informed approach

GCMs often exhibit large biases in near-surface wind speed over complex coastal terrain such as Northwest Africa, where boundary-layer processes, coastal jets, and topographic channelings are poorly resolved. We therefore use the observed relationship between the meridional SST gradient and the north–south wind differential as a physically constrained transfer function. We compared the direct CMIP6 wind projections with the SST-gradient-informed projection. The direct CMIP6 winds agree in sign (decline in northern coastal winds) but show a larger inter-model spread. The SST-gradient approach provides a more observationally anchored central estimate, while the direct CMIP6 winds provide an estimate of structural uncertainty.

2.6 Risk Thresholds

Projections were evaluated by the year when WPD crosses three critical thresholds:

- 50% of the 2020 baseline (resource halving)
- 150 W m^{-2} (commercial viability limit [20])
- 50 W m^{-2} (near-zero operational threshold)

2.7 Uncertainty Quantification

Uncertainty was decomposed into three primary components following the framework established in the parent thesis [26, Ch. 4, Section 4.7.1]:

- Model uncertainty: Represented by the spread across the five CMIP6 models used in the SST-gradient-informed projections (Table 1). This component is largest for inland (±8.1%) and northern (±6.2%) sites, reflecting greater divergence in how models represent topographic effects and cyclone activity.
- Scenario uncertainty: Represented by the range across SSP1-2.6, SSP2-4.5, and SSP5-8.5. This component (±4–6%) is policy-relevant: it represents the uncertainty that can be reduced through emissions mitigation.
- Internal variability: Represented by the standard deviation of decadal means within each scenario. This component is smallest in the southern region (±2.8%) and largest in inland sites (±4.8%).

Total uncertainty was summarized using a root-sum-square (RSS) formulation of the three components. This decomposition is used as an approximate characterization of the relative contributions of model, scenario, and internal variability and assumes negligible covariance among the components; if the components are correlated, the total uncertainty may be overestimated or underestimated. The resulting values should therefore be interpreted as an uncertainty summary rather than as strictly independent probability bounds. Table 4 presents the uncertainty decomposition for each region under SSP5-8.5.

.3. Results

3.1 Validation of Baseline Data

All validation statistics were computed on deseasonalised monthly anomalies, in which the seasonal cycle was removed by subtracting the long-term monthly climatology (1981–2020) from each time series. This step was applied specifically for the model validation to avoid spurious correlations driven by the shared annual cycle; it was not applied to the Random Forest attribution analysis in Section 2.3, which uses monthly mean data at 100 m with the seasonal cycle retained.

Table 2. Validation of ERA5 against NASA POWER, MERRA-2, and NOAA OISST using deseasonalised monthly anomalies (1981–2020). R^2 = coefficient of determination; RMSE = root mean square error; MBE = mean bias error.

Variable	Dataset	R^2	RMSE	MBE
Wind speed (north)	NASA POWER	0.72	0.48 m s^{-1}	+0.04 m s^{-1}
Wind speed (south)	NASA POWER	0.76	0.42 m s^{-1}	−0.03 m s^{-1}
Wind speed (north)	MERRA-2	0.70	0.51 m s^{-1}	+0.07 m s^{-1}
SST (Mediterranean)	NOAA OISST	0.89	0.31 °C	+0.06 °C
SST (Canary)	NOAA OISST	0.88	0.29 °C	−0.03 °C

3.2 Observed Asymmetry and Trends

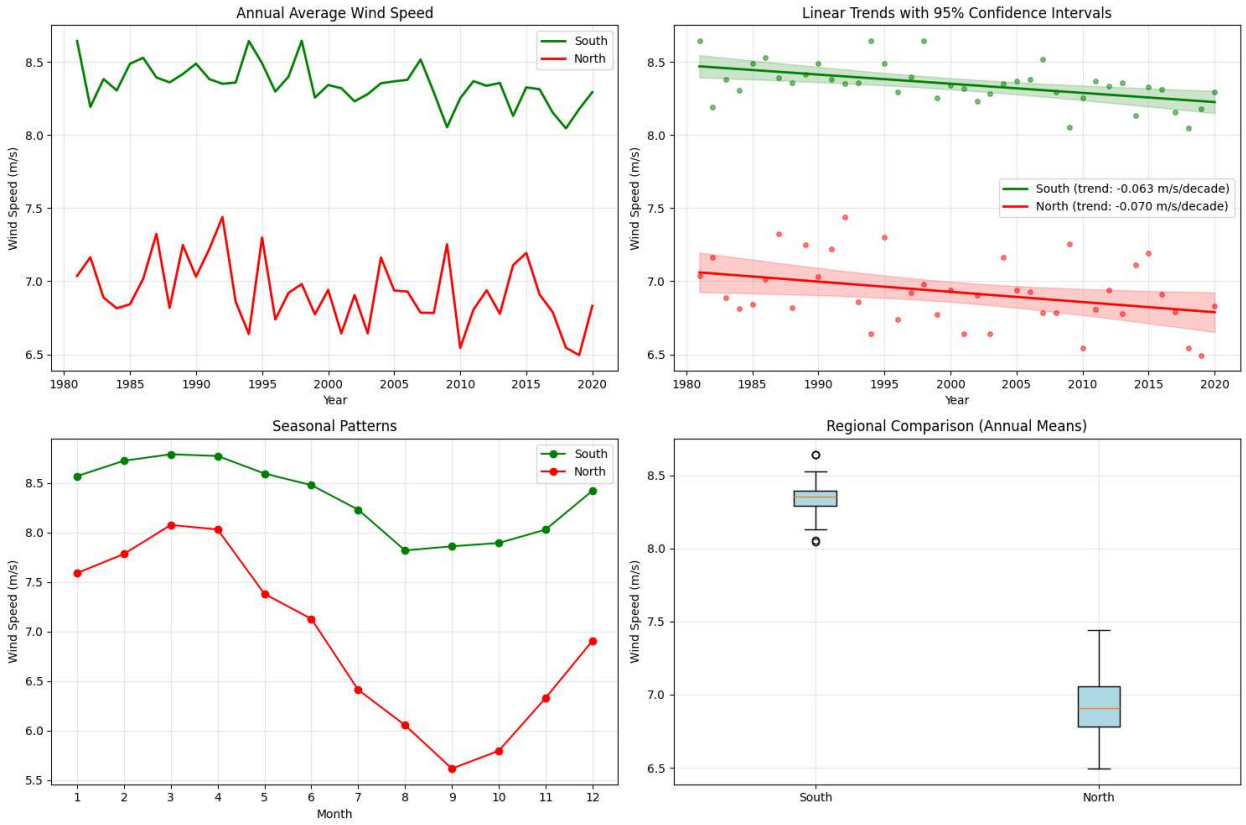


Figure 2. Historical wind speed characteristics for northern (red) and southern (green) coastal Morocco (1981–2020). **(a)** Annual mean wind speed time series. **(b)** Linear trends in annual mean wind speed with 95% confidence intervals; shaded bands represent the confidence intervals. **(c)** Monthly climatology of wind speed (seasonal cycle) over the 12

months. **(d)** Regional comparison of annual mean wind speed shown as boxplots; boxes represent the interquartile range, whiskers extend to the 5th–95th percentiles, horizontal lines indicate medians, and black diamonds indicate means. All wind speeds are in m s^{-1}.

Figure 2 presents the historical wind speed characteristics for both regions: (a) the annual mean time series (1981–2020), (b) linear trends with 95% confidence intervals, (c) the monthly seasonal cycle over the 12 months, and (d) a regional comparison of annual means shown as boxplots. The southern coast (green) consistently exceeds the northern coast (red) in annual mean wind speed. Consistently, the southern coast exhibits a mean wind power density of 518 $W \cdot m^{-2}$, approximately 1.6 times higher than the northern coast (324 $W \cdot m^{-2}$). Both regions show statistically significant declining trends (*p* < 0.05), but the northern rate (−0.0311 m s^{-1} per decade) is 11% faster than that of the south (−0.028 m s^{-1} per decade). Inter-annual variability, measured by the standard deviation of annual means, is 1.9 times larger in the north (σ_north = 0.41 m s^{-1}; σ_south = 0.22 m s^{-1}).

3.2.1 Capacity Factor Implications

The asymmetry in wind power density translates directly into operational energy metrics. Using the power curve methodology for modern multi-megawatt turbines (3–4 MW class, cut-in speed $3\ m \cdot s^{-1}$, cut-out $25\ m \cdot s^{-1}$) detailed in the parent thesis [26, Ch. 3], the southern region maintains a capacity factor of 38% by 2100 under SSP5-8.5, remaining above the 35% high-viability threshold defined by IRENA [20].

In contrast, the northern region's capacity factor declines to 25% by 2100 under the same scenario, crossing below the 30% economic bankability threshold for utility-scale projects without subsidies or favorable financing. This 13-percentage-point gap in capacity factor represents a proportional reduction in annual energy yield, with cumulative revenue losses exceeding €100 million over a 25-year project lifetime for a typical 100 MW wind farm [26, Ch. 4].

3.3 Attribution to SST Gradient

The Random Forest model, trained on ERA5 monthly mean data at 100 m with the seasonal cycle retained (1981–2020), explained 74% of the variance in the modelled north–south wind speed differential (Δv), with a test R^2 of 0.72. Permutation importance identified Mediterranean SST (0.343), Canary Current SST (0.338), and sea-level pressure gradient (0.319) as the principal predictors (Figure 3). The two SST predictors together accounted for approximately 68% of the total permutation importance (combined score = 0.681). This result indicates that the meridional SST contrast provides a substantial contribution to the statistical prediction of the modelled wind-speed differential. However, because the SST predictors are interrelated, their permutation importance should not be interpreted as independent causal contributions; it reflects predictive contribution within the model and is consistent with, though not equivalent to, a physical or mechanistic attribution. The proposed physical interpretation is further supported by the correlation analysis (Figure

4), in which Δv exhibits a strong negative correlation with ΔSST (*r* = −0.78) and a strong positive correlation with ΔP (*r* = 0.81). Other atmospheric drivers, including large-scale circulation modes such as the North Atlantic Oscillation, may also contribute to the modelled variability. Error bars in Figure 3 represent ±1 standard deviation across permutation iterations; the dashed red line indicates the baseline importance under random shuffling (*p* = 0.333).

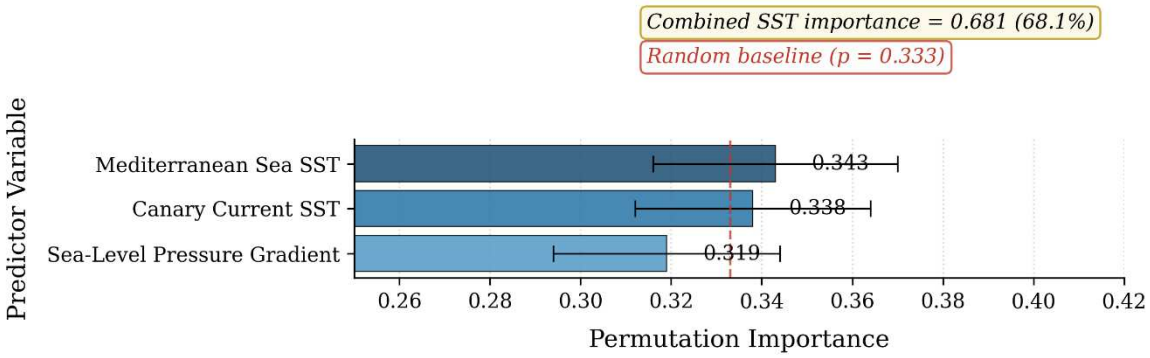


Figure 3. Permutation importance scores from Random Forest regression identifying Mediterranean SST, Canary Current SST, and sea-level pressure gradient as the dominant predictors of the modelled north–south wind speed differential. The model was trained on ERA5 monthly mean data at 100 m with the seasonal cycle retained (1981–2020). Error bars represent ±1 standard deviation across permutation iterations. The dashed red line indicates baseline importance under random shuffling (*p* = 0.333). Numeric values on the bars are the permutation importance scores; the two SST predictors jointly account for approximately 68% of the total permutation importance. This value reflects predictive contribution within the model and is consistent with, though not equivalent to, a physical or mechanistic attribution.

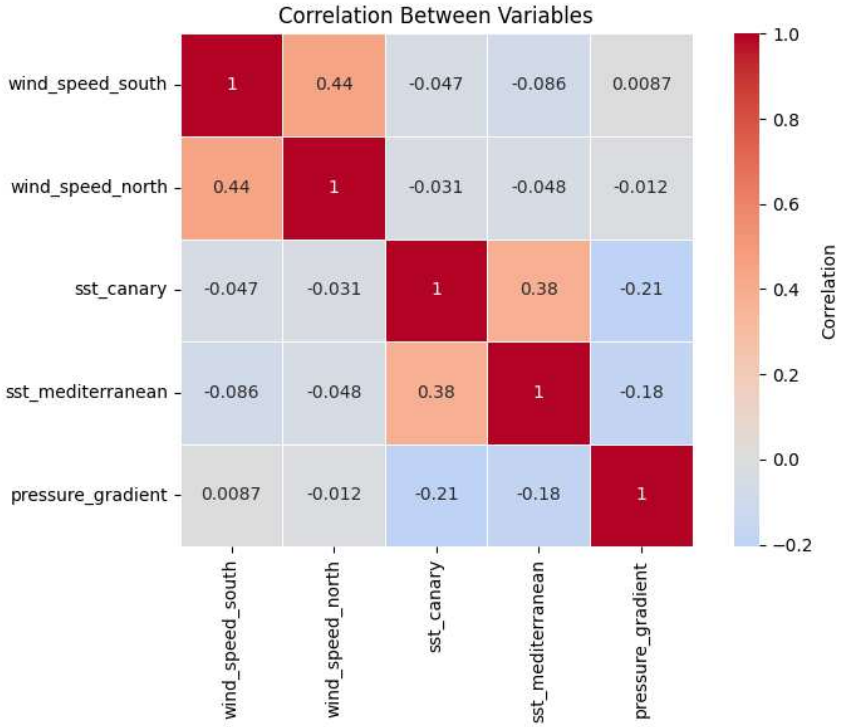


Figure 4. Correlation matrix showing relationships among Mediterranean SST, Canary Current SST, pressure gradient, and north–south wind speed difference. Values are Pearson correlation coefficients.

3.3.1 Physical mechanism

The statistical link between the SST gradient and the modelled north–south wind speed differential is consistent with a well-documented physical mechanism, which can be summarised as follows:

1. Differential warming: The Mediterranean Sea warms faster than the upwelling-cooled Canary Current system.
2. Pressure-gradient weakening: This differential warming is associated with a reduction in the meridional sea-level pressure gradient across Northwest Africa.
3. Wind forcing: The weakened pressure gradient is consistent with reduced geostrophic wind forcing, disproportionately affecting the northern coast, which is more directly coupled to Mediterranean low-pressure systems.

The proposed mechanism is supported by the Random Forest attribution (Section 3.3), the correlation structure (Figure 4), and the physical reasoning documented in the literature [21]. Nonetheless, other factors may also contribute to the observed spatial variation, including large-scale circulation variability (e.g., the North Atlantic Oscillation), topographic effects, and synoptic-scale disturbances. The correlation of -0.78 between Δv and ΔSST supports a robust statistical and physical link, but does not by itself constitute proof of a unique mechanism, and we do not claim a deterministic relationship.

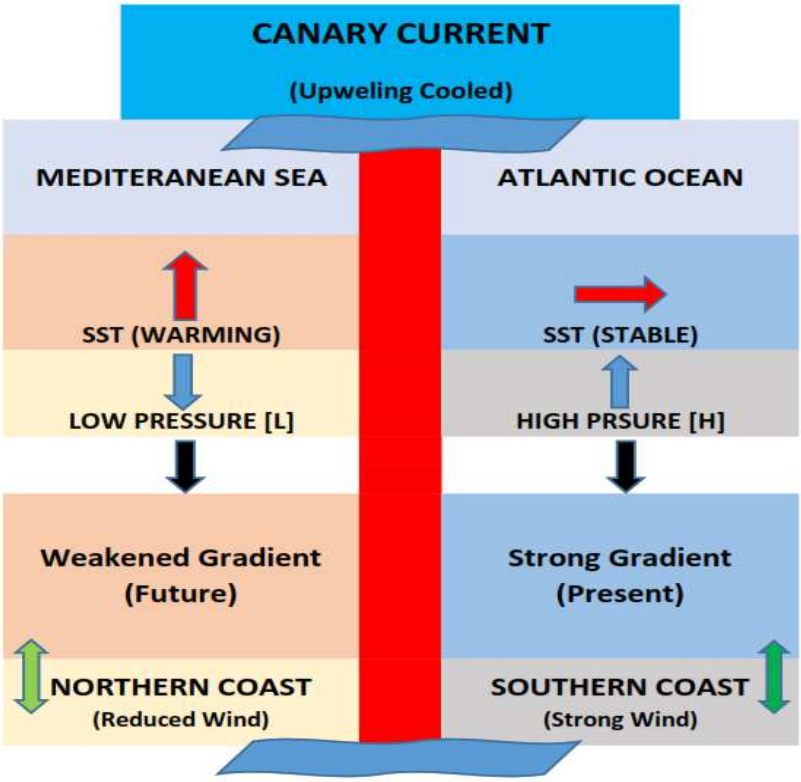


Figure 5. Conceptual model of the proposed mechanism. The Mediterranean Sea warms faster than the upwelling-cooled Canary Current, reducing the meridional SST gradient. This is associated with a weakened sea-level pressure gradient (low pressure over the Mediterranean, high pressure over the Atlantic) and is consistent with reduced geostrophic wind forcing along the northern coast. The figure shows the present strong gradient and the future weakened gradient, together with the contrasting wind response along the northern and southern coasts.

3.4 Multi-Model Projections

The four constrained models produce a range of estimated threshold-crossing periods for the northern coast under SSP5-8.5 (Table 3). The quadratic model yields the earliest estimate (2005–2025), while the logistic and CMIP6-informed models place the crossing period later (2015–2040 and 2020–2045, respectively). Two important caveats apply to the interpretation of these values.

First, the constrained linear, logistic, and quadratic models were fitted to the historical period (1981–2020) and then extended. Their threshold-crossing estimates therefore partly reflect **extrapolation of the fitted historical trend**, and the early years in these rows (2005–2015) should not be read as future projections. They indicate the period during which the historical trend, if continued, would have crossed the 150 $W \cdot m^{-2}$ threshold. The **future projection period in this study begins in 2020**.

Second, the values in Table 3 are **model-derived estimates, not confirmed future dates**, and the spread across the four models reflects methodological uncertainty rather than a precise forecast. The CMIP6-informed piecewise model, being driven purely by future projections of the SST

gradient, yields the estimate that is most directly interpretable as a future threshold-crossing period, and places the crossing in the 2020–2045 window.

The four models differ in structure rather than in claimed realism: the constrained linear model uses a constant trend with a physical floor; the logistic model produces an asymptotic decline constrained by a prescribed lower bound; the quadratic model allows for an accelerating decline; and the CMIP6-informed piecewise model scales the historical trend by projected SST-gradient change. The spread across these structures provides a bounded range of plausible outcomes rather than a single deterministic forecast.

Table 3. Model-estimated crossing periods for the 150 $W \cdot m^{-2}$ economic-viability threshold in the northern coastal region under SSP5-8.5, based on four constrained projection approaches.

Model	Core Principle	Estimated Threshold-Crossing Period	Interpretation
Constrained linear	Constant historical trend with physical floor	2008–2032 *(extrapolated from the historical trend)*	The historical trend, if continued, would cross the threshold within this window
Logistic (sigmoid)	Asymptotic decline constrained by a prescribed lower bound	2015–2040 (median 2028) *(extrapolated from the historical trend)*	Bounded asymptotic decline
Quadratic	Allows for acceleration ($\beta_2 < 0$, *p* = 0.03)	2005–2025 *(extrapolated from the historical trend)*	Suggests potential rapid near-term decline
CMIP6-informed piecewise	Trend scaled by projected SST-gradient change	2020–2045	The only approach driven purely by future projections

Note: Crossing periods derived from fitted historical relationships should not be interpreted as deterministic forecasts; they represent the range of threshold-crossing times implied by the respective model structures. β_2 is the quadratic coefficient in equation (4). Early values (before 2020) arise from extrapolation of the fitted historical trend and are not future projections.

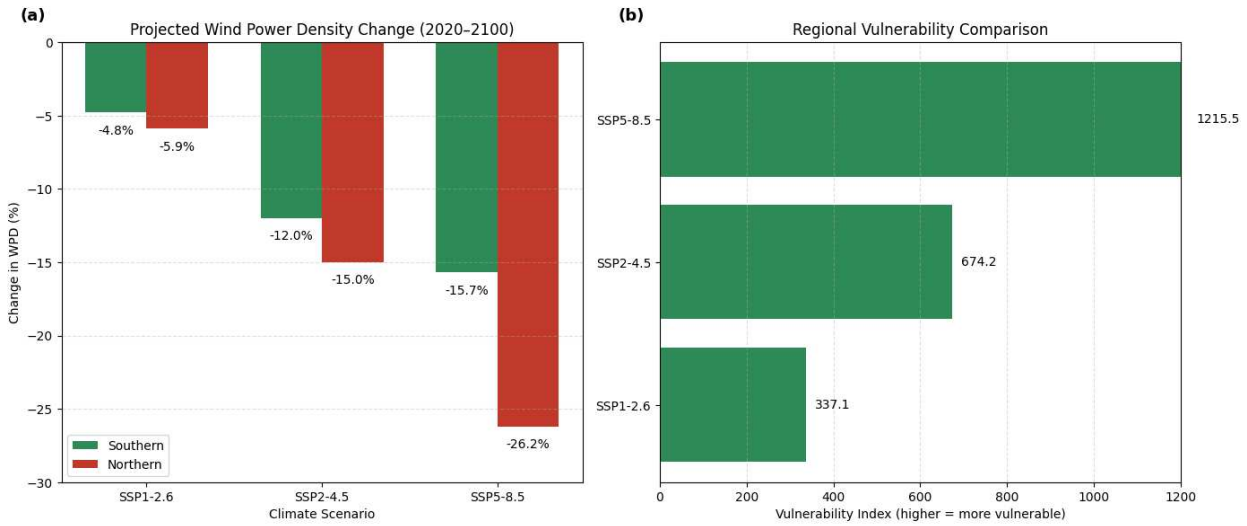


Figure 6. Projected wind power density change and regional vulnerability under three SSP scenarios. **(a)** Projected percentage change in wind power density by 2100 relative to the 2020 baseline, for the northern (red) and southern (green) coastal regions under SSP1-2.6, SSP2-4.5, and SSP5-8.5. **(b)** Regional vulnerability comparison showing the aggregate vulnerability index for each SSP scenario as horizontal bars (x-axis: 0–1200; higher values indicate greater vulnerability).

3.4.1 Comparison with direct CMIP6 wind projections

To assess whether the SST-gradient-informed approach is consistent with the direct climate-model response, we compared the sign and magnitude of projected northern-coast wind changes from the two approaches. The direct CMIP6 simulations generally reproduce a decline in northern coastal wind resources, but exhibit a larger inter-model spread than the SST-gradient-informed estimates. This agreement in the direction of change supports the consistency of the two approaches, while the larger spread of the direct simulations highlights structural uncertainty associated with the representation of near-surface coastal winds. Accordingly, the SST-gradient-informed estimates are interpreted as an observationally anchored projection rather than as a replacement for direct CMIP6 wind simulations.

The quadratic model's statistically significant negative acceleration coefficient $\beta_2 < 0$ (*p* = 0.03) indicates that wind power density may decline at an accelerating rate, bringing the 150 $W \cdot m^{-2}$ viability threshold forward by approximately 5–10 years relative to linear or logistic projections. For energy planners, this acceleration risk implies that mid-century resource assessments based on linear trends may substantially overestimate future wind availability.

3.5 Uncertainty Decomposition

Following the framework in Section 2.7, Table 4 presents the uncertainty decomposition for the four regions of the wider site network under SSP5-8.5. The two coastal zones that form the primary

focus of this paper are Northern and Southern; the Central Coastal and Inland regions are included for completeness. Total uncertainty ranges from ±5.9% (southern) to ±10.8% (inland), with model uncertainty dominating for inland and northern regions. Figure 6b provides a complementary regional vulnerability comparison, summarising the composite vulnerability index for the three SSP scenarios.

Table 4. Uncertainty decomposition for projected WPD decline by region (SSP5-8.5, 2100). RSS = root sum square.

Region	Model Uncertainty (%)	Scenario Uncertainty (%)	Internal Variability (%)	Total Uncertainty (RSS, %)
Southern	±3.2	±4.1	±2.8	±5.9
Central	±4.5	±5.2	±3.4	±7.6
Northern	±6.2	±5.8	±4.1	±9.3
Inland	±8.1	±5.4	±4.8	±10.8

Note: Values represent the standard deviation of projected WPD declines across ensemble members (model uncertainty), across SSP scenarios (scenario uncertainty), and across decadal means (internal variability). Total uncertainty is calculated as the root sum square (RSS) of the three components. This provides an approximate characterization of uncertainty and assumes negligible covariance among the individual components; the total values should therefore be interpreted as indicative rather than exact [26, Ch. 4, Section 4.7.1]. The Southern and Northern rows correspond to the two coastal zones that form the primary focus of this paper. The Central and Inland rows are retained from the wider site network analysed in the parent study [26] for completeness of the uncertainty decomposition.

4. Discussion

4.1 Physical Mechanism and Validation

The results are consistent with a coherent physical mechanism linking regional ocean warming to coastal wind power declines, as described in Section 3.3.1 and supported by the literature. Amplified warming of the Mediterranean Sea relative to the upwelling-stabilized Canary Current weakens the meridional pressure gradient across Northwest Africa [21]. This weakening disproportionately reduces geostrophic wind forcing in the northern coastal region, which is more directly coupled to Mediterranean low-pressure systems than its southern counterpart.

The enhanced inter-annual variability in the north is in line with its heightened sensitivity to regional atmospheric oscillations and transient synoptic forcing. The strong agreement between ERA5-derived SST gradient and independent NASA/NOAA SST products reinforces the physical credibility of this mechanism (Figure 5), advancing attribution beyond purely statistical association toward a process-based interpretation.

The projected decline in Morocco's coastal wind resources is not spatially uniform, and this asymmetry cannot be explained by climate change scenarios alone. Global climate models consistently project a general reduction in near-surface wind speeds under warming, but the magnitude of that reduction in Morocco is region-dependent and depends on the way in which large-scale circulation interacts with the regional boundary-layer regime. In this study, the northern coast — influenced by Mediterranean synoptic systems, coastal jets, and boundary-layer processes through the Strait of Gibraltar — is projected to lose a substantially larger fraction of its wind power density than the southern coast (approximately 26% versus 16% under SSP5-8.5), which is anchored to the persistent Atlantic trade winds. The Random Forest attribution and the physical mechanism presented in Section 3.3.1 together point to the meridional SST gradient between the Mediterranean Sea and the Canary Current as the dominant regional modulator of that asymmetry. As the Mediterranean warms faster than the upwelling-cooled Canary Current, the regional pressure gradient weakens, boundary-layer stability increases, and the northern coastal wind regime is disproportionately affected. This is a regional mechanism operating on top of the global warming signal, not a substitute for it. The implication is that future wind-energy assessments for Morocco — and, by extension, for similar coastal regions in Northwest Africa — should not rely on climate change scenarios alone, but should explicitly account for the regional air–sea interaction and boundary-layer dynamics that shape the spatial pattern of the decline.

4.2 Methodological Uncertainty and Multi-Model Framework

This study indicates that the choice of projection methodology introduces a 10–20 year uncertainty band in risk assessment timelines, a range comparable to the "time of emergence" uncertainty documented in broader climate science [22]. Although prior work has critiqued the use of linear extrapolation in wind resource assessment [3], the present analysis offers a quantified assessment of how alternative model structures influence economically critical projections.

To address this, a four-model ensemble was developed, each variant targeting a distinct methodological concern while collectively transforming uncertainty into a quantifiable risk spectrum. The logistic model produces an asymptotic decline constrained by a prescribed lower bound, thereby precluding negative wind speeds. The quadratic model formalizes testing for acceleration risk; the significant negative coefficient (*p* = 0.03) indicates that an accelerating decline cannot be ruled out. The CMIP6-informed model scales the historical ERA5-derived trend by the projected change in the SST gradient, anchoring the projection to the regional mechanism discussed in Section 3.3.1. Together, these models provide planners with a distribution of outcomes rather than a single

deterministic forecast, reframing methodological uncertainty as a structured characterization of alternative futures.

The uncertainty decomposition (Table 4) further refines this framework by quantifying the relative contributions of model, scenario, and internal variability. For energy planning, this implies:

- **Short-term investments (to 2040):** Focus on adaptive management that can respond to observed variability, as internal variability dominates near-term projections.
- **Long-term infrastructure (beyond 2070):** Scenario uncertainty dominates — decisions should be robust across the range of projections considered here.

The four-model framework captures structural uncertainty in the projection methods; it does not capture all sources of uncertainty, such as large-scale circulation variability, topographic effects, or synoptic-scale disturbances, which may additionally modulate regional wind resources.

4.3 Policy Implications

The asymmetric, model-informed risks identified in this study suggest that climate risk should be considered explicitly in the planning and assessment of future wind-energy projects in Morocco. The considerations below are intended as climate-risk planning inputs, rather than as fixed engineering or financial requirements, which lie beyond the scope of this study.

Immediate considerations (2024–2030):

- **Development of the southern coast.** The southern region retains the highest wind power density by 2100 under all scenarios (approximately 437 $W \cdot m^{-2}$ under SSP5-8.5, with a capacity factor of about 38%) and remains the most climate-resilient zone for wind-energy investment. Consideration could be given to prioritising permitting and grid connection in the Tarfaya and Akhfener zones, together with feasibility studies for offshore wind potential in the adjacent southern Atlantic.
- **Climate-risk assessment in project planning.** New wind-energy projects, particularly in the northern coastal zone, may benefit from a climate-risk assessment based on multi-model ensemble projections rather than on historical wind statistics alone. Such assessments may consider the full range of SSP scenarios and the associated uncertainty envelope described in Section 3.5.
- **Adaptive planning frameworks.** Because the projected decline in the northern coastal region is larger, earlier, and more variable than in the south, the northern zone may be best managed through adaptive planning pathways that can be revised as observations accumulate, rather than through a single fixed design assumption. This is consistent with standard decision-making under deep uncertainty.
- **Transmission infrastructure between south and north.** The resilience of the southern coast offers a strategic opportunity to supply northern demand centres through expanded

south–north transmission corridors, thereby reducing the exposure of the national grid to northern coastal resource decline. This warrants consideration in future grid planning.

- **Periodic monitoring protocol.** The SST gradient between the Mediterranean and the Canary Current is a physically interpretable indicator of the mechanism discussed in Section 3.3.1. Monitoring this gradient, together with real-time wind observations, may provide an early-warning signal that could inform periodic reassessment of resource projections.

Medium-term considerations (2030–2050):

- **Region-specific adaptation pathways.** For the northern coast, consideration could be given to periodic reassessment of long-term investments and to technology-neutral adaptation strategies (e.g., advanced forecasting, improved turbine selection). For the central coast, integrated wind and solar planning may be beneficial. For inland sites, a full techno-economic reassessment is warranted.
- **Diversification of the renewable portfolio.** Because wind resources in northern and inland Morocco are projected to decline, while solar resources may remain stable or improve, national planning may benefit from explicit consideration of portfolio diversification across wind, solar, storage, and, where feasible, green hydrogen. This could reduce the exposure of the energy system to any single resource trajectory.
- **Improved forecasting capability.** Increased interannual variability and more frequent low-wind events in the northern region (projected to rise by approximately 7.8 percentage points under SSP5-8.5) increase the value of improved short-term and seasonal forecasting for grid operation and reserve planning.
- **Climate uncertainty in financial planning.** Public financing and risk-sharing instruments may benefit from incorporating the uncertainty envelope presented in this study, rather than relying on single deterministic projections. The development of appropriate climate risk instruments is a matter for financial institutions and lies beyond the scope of this study, but the analytical framework presented here provides a basis for such assessments.

Long-term considerations (post-2050):

- **Adaptive governance.** A permanent interministerial committee on climate resilience in energy, with a mandate for periodic (five-year) review of climate projections and adaptation strategies, would institutionalise the adaptive approach recommended here and embed the multi-model framework of this study into Morocco's National Energy Strategy. This warrants consideration as a governance mechanism.
- **Global mitigation.** The difference between the SSP1-2.6 and SSP5-8.5 pathways reaches 87 $W \cdot m^{-2}$ in national average wind power density by 2100 [26, Ch. 4]. This gap is not a technical abstraction but a direct determinant of national infrastructure viability,

cumulative revenue, and long-term energy security. Strengthening global mitigation directly protects Morocco's domestic wind resource.

These considerations should be interpreted as climate-risk planning inputs rather than as fixed engineering or financial requirements, because detailed techno-economic optimization was beyond the scope of the present study.

5. Conclusion

This study demonstrates that wind power density decline along Morocco's coastal regions is spatially asymmetric, with a substantially larger decline in the northern coastal region than in the southern region across all three SSP scenarios. The asymmetry is consistent with a plausible physical mechanism driven by differential ocean warming, as described in Section 3.3.1 and supported by independent literature on Mediterranean–Atlantic air–sea interaction. The Random Forest attribution indicates that the two SST predictors jointly account for approximately 68% of the total permutation importance in the modelled north–south wind speed differential, but this statistical result supports rather than proves the proposed mechanism; other factors, including large-scale circulation variability, topography, and synoptic-scale disturbances, may also contribute.

The estimated timing of the 150 $W \cdot m^{-2}$ threshold crossing depends on both the projection method and the emission scenario. The four constrained models yield crossing periods ranging from the historical-fit window (2005–2032, partly extrapolated from the historical trend) to the future-projection window (2020–2045), and the CMIP6-informed piecewise model — being driven purely by future projections of the SST gradient — yields the estimate that is most directly interpretable as a future threshold-crossing period. **The projected threshold-crossing times should therefore be interpreted as ranges of plausible outcomes rather than as deterministic dates.** The CMIP6-informed projections should be interpreted within the framework of model structural uncertainty, since GCMs often exhibit biases in near-surface wind over complex coastal terrain, and the SST-gradient-informed approach is used here to provide a more physically constrained and observationally anchored central estimate.

The northern coastal wind resource is exposed to considerably higher and potentially nearer-term climate risk than the southern resource. The projected 15–35-year lead time in loss of economic viability in the north should be interpreted as a risk envelope rather than a deterministic forecast. Adoption of an ensemble-based planning paradigm can transform climatological risk into strategic opportunity, enabling informed investment decisions, grid modernization, and technological adaptation to safeguard Morocco's energy transition.

Central policy message. This study reinforces a critical finding from the parent thesis [26]: the choice between a high-emission future (SSP5-8.5) and a sustainable one (SSP1-2.6) is not merely a global policy abstraction but a direct determinant of Morocco's domestic wind resource.

The difference in national average wind power density between these pathways reaches 87 $W \cdot m^{-2}$ by 2100 [26, Ch. 4]. This gap represents not a technical metric but billions of euros in cumulative revenue losses, thousands of jobs, and the substance of Morocco's energy independence. Climate action and energy security are intrinsically linked: ambitious global mitigation directly protects national infrastructure.

Further work incorporating longer observational records, additional atmospheric predictors, direct wind-farm measurements, higher-resolution regional climate simulations, and detailed techno-economic analysis would help reduce the remaining uncertainties and improve the practical applicability of the projections.

6. Acknowledgements

The authors thank the Copernicus Climate Change Service, NASA Langley Research Center, and NOAA for providing open access to reanalysis and observational data.

7. References

[1] Ministère de l'Energie, des Mines et de l'Environnement. Stratégie énergétique nationale: Horizon 2030. Royaume du Maroc, 2020.
[2] Zeng Z, Ziegler AD, Searchinger T, et al. A reversal in global terrestrial stilling and its implications for wind energy production. Nat. Clim. Change, 2019, 9(12): 979–985. doi: 10.1038/s41558-019-0622-6.
[3] Pryor SC, Barthelmie RJ, Bukovsky MS, et al. Climate change impacts on wind power generation. Nat. Rev. Earth Environ., 2020, 1(12): 627–643. doi: 10.1038/s43017-020-0101-7.
[4] Marullo S, Serva F, Iacono R, et al. Mediterranean Sea surface warming 1982–2020: A revised assessment using satellite data. Remote Sens., 2021, 13(16): 3264. doi: 10.3390/rs13163264.
[5] Jiang Q, Wang S, Zhang Y, et al. Mediterranean warming and wind patterns: Impacts on coastal energy resources. Clim. Dyn., 2020, 54(3): 1129–1144. doi: 10.1007/s00382-019-05055-9.
[6] Hersbach H, Bell B, Berrisford P, et al. The ERA5 global reanalysis. Q. J. R. Meteorol. Soc., 2020, 146(730): 1999–2049. doi: 10.1002/qj.3803.
[7] NASA Prediction of Worldwide Energy Resources (POWER). Data Access Viewer. NASA Langley Research Center, 2023. Available at: https://power.larc.nasa.gov (accessed 15 March 2026).
[8] Gelaro R, McCarty W, Suárez MJ, et al. The Modern Era Retrospective Analysis for Research and Applications, Version 2 (MERRA-2). J. Clim., 2017, 30(14): 5419–5454. doi: 10.1175/JCLI-D-16-0758.1.
[9] Reynolds RW, Smith TM, Liu C, et al. Daily high-resolution-blended analyses for sea surface temperature. J. Clim., 2007, 20(22): 5473–5496. doi: 10.1175/2007JCLI1824.1.
[10] Chin TM, Vazquez-Cuervo J, Armstrong EM. GHRSST Level 4 analysis. NASA JPL, 2017. Available at: https://podaac.jpl.nasa.gov/dataset/ (accessed 15 March 2026).
[11] Kendall MG. Rank correlation methods. 4th ed. London: Charles Griffin, 1975.
[12] Sen PK. Estimates of the regression coefficient based on Kendall's tau. J. Am. Stat. Assoc., 1968, 63(324): 1379–1389. doi: 10.1080/01621459.1968.10480934.
[13] Breiman L. Random forests. Mach. Learn., 2001, 45(1): 5–32. doi: 10.1023/A:1010933404324.

[14] O'Neill BC, Tebaldi C, van Vuuren DP, et al. The Scenario Model Intercomparison Project (ScenarioMIP) for CMIP6. Geosci. Model Dev., 2016, 9(9): 3461–3482. doi: 10.5194/gmd-9-3461-2016.
[15] Danabasoglu G, Lamarque JF, Bacmeister J, et al. The Community Earth System Model version 2 (CESM2). J. Adv. Model. Earth Syst., 2020, 12(2): e2019MS001916. doi: 10.1029/2019MS001916.
[16] Mauritsen T, Bader J, Becker T, et al. Developments in the MPI-M Earth System Model version 1.2 (MPI-ESM1.2). J. Adv. Model. Earth Syst., 2019, 11(4): 998–1038. doi: 10.1029/2019MS001894.
[17] Sellar AA, Jones CG, Mulcahy JP, et al. UKESM1: Description and evaluation of the UK Earth System Model. J. Adv. Model. Earth Syst., 2019, 11(12): 4513–4558. doi: 10.1029/2019MS001739.
[18] Tatebe H, Ogura T, Nitta T, et al. Description and basic evaluation of the MIROC6 climate model. J. Adv. Model. Earth Syst., 2019, 11(7): 2153–2213. doi: 10.1029/2019MS001682.
[19] Dunne JP, Horowitz LW, Adcroft AJ, et al. The GFDL Earth System Model version 4.1 (GFDL-ESM4.1). J. Adv. Model. Earth Syst., 2020, 12(10): e2019MS002096. doi: 10.1029/2019MS002096.
[20] IRENA. Renewable power generation costs in 2020. International Renewable Energy Agency, 2021. Available at: https://www.irena.org/publications/2021/Jun/Renewable-PowerCosts-in-2020.
[21] Patricola CM, Chang P. Structure and dynamics of the Atlantic-Mediterranean interface. J. Clim., 2017, 30(9): 3105–3122. doi: 10.1175/JCLI-D-16-0425.1.
[22] Hawkins E, Sutton R. Time of emergence of climate signals. Geophys. Res. Lett., 2012, 39(1): L01702. doi: 10.1029/2011GL050087.
[23] IRENA. Renewable energy prospects: Morocco. International Renewable Energy Agency, 2022. Available at: https://www.irena.org/publications/2022/Mar/Renewable-Energy-Prospects-Morocco.
[24] Benazzouz A, Mabchour H, El Aouad M, et al. Offshore wind energy resource in the Kingdom of Morocco. J. Mar. Sci. Eng., 2021, 9(1): 31. doi: 10.3390/jmse9010031.
[25] Emeis S. Wind energy meteorology: Atmospheric physics for wind power generation. 2nd ed. Springer, 2018. doi: 10.1007/978-3-319-72859-9.
[26] Badry YS. Assessment of Climate Change Impact on Potential Wind Power Using Regional Climate Model (CORDEX) in Morocco [PhD thesis]. Cairo University; 2026.

Ethics and Disclosures

Authorship Statement: All authors made substantial contributions to the conception and design of the work, data acquisition and analysis, and drafting of the manuscript. All authors approved the submitted version and agree to be personally accountable for their contributions.

Conflict of Interest: The authors declare that they have no competing interests.

Data Availability: ERA5 reanalysis data are publicly available from the Copernicus Climate Data Store (https://cds.climate.copernicus.eu). NASA POWER data are available from the NASA Langley Research Center (https://power.larc.nasa.gov). CMIP6 model outputs are accessible via the Earth System Grid Federation (https://esgf-node.llnl.gov). Derived datasets and analysis code are available from the corresponding author upon reasonable request.

Declaration of AI and Software Assistance: During the preparation of this manuscript, the authors used DeepSeek, an artificial intelligence language model, for language refinement, grammar checking, and editorial assistance in structuring the manuscript. The AI tool was not used for data analysis, interpretation of results, or the design of the multi-model projection framework. All technical content, data analysis, interpretation, results, and final intellectual contributions remain the sole responsibility of the authors.

Foundation item: This research received no specific grant from any funding agency in the public, commercial, or not-for-profit sectors.